The Astrophysical Journal, 831:185 (8pp), 2016 November 10 doi:10.3847/0004-637X/831/2/185
© 2016. The American Astronomical Society. All rights reserved.

THE *NuSTAR* EXTRAGALACTIC SURVEYS: THE NUMBER COUNTS OF ACTIVE GALACTIC NUCLEI AND THE RESOLVED FRACTION OF THE COSMIC X-RAY BACKGROUND

F. A. Harrison[1], J. Aird[2,3], F. Civano[4], G. Lansbury[3], J. R. Mullaney[5], D. R. Ballantyne[6], D. M. Alexander[3], D. Stern[7], M. Ajello[8], D. Barret[9], F. E. Bauer[10,11,12], M. Baloković[1], W. N. Brandt[13,14,15], M. Brightman[1], S. E. Boggs[16], F. E. Christensen[17], A. Comastri[18], W. W. Craig[16,19], A. Del Moro[3], K. Forster[1], P. Gandhi[20], P. Giommi[21], B. W. Grefenstette[1], C. J. Hailey[22], R. C. Hickox[23], A. Hornstrup[17], T. Kitaguchi[24], J. Koglin[25], B. Luo[13,14,15], K. K. Madsen[1], P. H. Mao[1], H. Miyasaka[1], K. Mori[22], M. Perri[21,26], M. Pivovaroff[19], S. Puccetti[21,26], V. Rana[1], E. Treister[27], D. Walton[1,7], N. J. Westergaard[17], D. Wik[28], L. Zappacosta[26], W. W. Zhang[28], and A. Zoglauer[16]

[1] Cahill Center for Astronomy and Astrophysics, California Institute of Technology, Pasadena, CA 91125
[2] Institute of Astronomy, University of Cambridge, Madingley Road, Cambridge, CB3 0HA, UK
[3] Centre of Extragalactic Astronomy, Department of Physics, Durham University, Durham, DH1 3LE, UK
[4] Yale Center for Astronomy and Astrophysics, 260 Whitney Avenue, New Haven, CT 06520, USA
[5] The Department of Physics and Astronomy, The University of Sheffield, Hounsfield Road, Sheffield S3 7RH, UK
[6] Center for Relativistic Astrophysics, School of Physics, Georgia Institute of Technology, Atlanta, GA 30332, USA
[7] Jet Propulsion Laboratory, California Institute of Technology, 4800 Oak Grove Drive, Pasadena, CA 91109, USA
[8] Department of Physics and Astronomy, Clemson University, Kinard Lab of Physics, Clemson, SC 29634-0978, USA
[9] Universite de Toulouse; UPS-OMP; IRAP; Toulouse, France & CNRS; Institut de Recherche en Astrophysique et Planétologie; 9 Av. colonel Roche, BP 44346, F-31028 Toulouse cedex 4, France
[10] Instituto de Astrofísica, Facultad de Física, Pontificia Universidad Catòlica de Chile, 306, Santiago 22, Chile
[11] Millennium Institute of Astrophysics, Santiago, Chile
[12] Space Science Institute, 4750 Walnut Street, Suite 205, Boulder, CO 80301, USA
[13] Department of Astronomy and Astrophysics, The Pennsylvania State University, 525 Davey Lab, University Park, PA 16802, USA
[14] Institute for Gravitation and the Cosmos, The Pennsylvania State University, University Park, PA 16802, USA
[15] Department of Physics, The Pennsylvania State University, University Park, PA 16802, USA
[16] Space Sciences Laboratory, University of California, Berkeley, CA 94720, USA
[17] DTU Space—National Space Institute, Technical University of Denmark, Elektrovej 327, DK-2800 Lyngby, Denmark
[18] INAF Osservatorio Astronomico di Bologna, via Ranzani 1, I-40127, Bologna, Italy
[19] Lawrence Livermore National Laboratory, Livermore, CA 94550, USA
[20] School of Physics & Astronomy, University of Southampton, Highfield, Southampton SO17 1BJ, UK
[21] ASI Science Data Center (ASDC), via del Politecnico, I-00133 Rome, Italy
[22] Columbia Astrophysics Laboratory, Columbia University, New York, NY 10027, USA
[23] Department of Physics and Astronomy, Dartmouth College, 6127 Wilder Laboratory, Hanover, NH 03755, USA
[24] Department of Physical Science, Hiroshima University, 1-3-1 Kagamiyama, Higashi-Hiroshima, Hiroshima 739-8526, Japan
[25] Kavli Institute for Particle Astrophysics and Cosmology, SLAC National Accelerator Laboratory, Menlo Park, CA 94025, USA
[26] INAF-Osservatorio Astronomico di Roma, via di Frascati 33, I-00078, Monte Porzio Catone, Italy
[27] Universidad de Concepciòn, Departamento de Astronomía, Casilla 160-C, Concepciòn, Chile
[28] NASA Goddard Space Flight Center, Greenbelt, MD 20771, USA

Received 2015 October 29; revised 2016 August 23; accepted 2016 August 24; published 2016 November 7

ABSTRACT

We present the 3–8 keV and 8–24 keV number counts of active galactic nuclei (AGNs) identified in the *Nuclear Spectroscopic Telescope Array* (*NuSTAR*) extragalactic surveys. *NuSTAR* has now resolved 33%–39% of the X-ray background in the 8–24 keV band, directly identifying AGNs with obscuring columns up to $\sim 10^{25}$ cm^{-2}. In the softer 3–8 keV band the number counts are in general agreement with those measured by *XMM-Newton* and *Chandra* over the flux range $5 \times 10^{-15} \lesssim S(3\text{–}8\ \mathrm{keV})/\mathrm{erg\ s^{-1}\ cm^{-2}} \lesssim 10^{-12}$ probed by *NuSTAR*. In the hard 8–24 keV band *NuSTAR* probes fluxes over the range $2 \times 10^{-14} \lesssim S(8\text{–}24\ \mathrm{keV})/\mathrm{erg\ s^{-1}\ cm^{-2}} \lesssim 10^{-12}$, a factor ∼100 fainter than previous measurements. The 8–24 keV number counts match predictions from AGN population synthesis models, directly confirming the existence of a population of obscured and/or hard X-ray sources inferred from the shape of the integrated cosmic X-ray background. The measured *NuSTAR* counts lie significantly above simple extrapolation with a Euclidian slope to low flux of the *Swift*/BAT 15–55 keV number counts measured at higher fluxes ($S(15\text{–}55\ \mathrm{keV}) \gtrsim 10^{-11}$ erg s^{-1} cm^{-2}), reflecting the evolution of the AGN population between the *Swift*/BAT local ($z < 0.1$) sample and *NuSTAR*'s $z \sim 1$ sample. CXB synthesis models, which account for AGN evolution, lie above the *Swift*/BAT measurements, suggesting that they do not fully capture the evolution of obscured AGNs at low redshifts.

Key words: galaxies: active – galaxies: nuclei – galaxies: Seyfert – surveys – X-rays: diffuse background – X-rays: galaxies

1. INTRODUCTION

A complete census of accreting supermassive black holes (SMBH) throughout cosmic time is necessary to quantify the efficiency of accretion, which is believed to drive the majority of SMBH growth (e.g., Soltan 1982; Yu & Tremaine 2002; Di Matteo et al. 2008, Merloni & Heinz 2008). X-ray emission is nearly universal from the luminous active galactic nuclei (AGNs) that signal the most rapid SMBH growth phases, making surveys in the X-ray band particularly efficient at identifying accreting SMBH. Unlike optical and infrared light, X-rays are not diluted by host-galaxy emission, which is

generally weak above ∼1 keV. X-rays are also penetrating, and hard ($\gtrsim$10 keV) X-rays are visible through columns up to $N_{\rm H} \sim 10^{25}\,{\rm cm}^{-2}$. For even higher columns, AGNs can be identified through scattered X-rays; though, the emission becomes progressively weaker with increasing columns.

Cosmic X-ray surveys with *Chandra* and *XMM-Newton* have provided measurements of the demographics of the AGN population and its evolution in the 0.1–10 keV band out to large cosmic distances (see Brandt & Alexander 2015, for a recent review). These surveys are sufficiently complete over a broad enough range of luminosity and redshift that many fundamental questions regarding AGN evolution can be addressed. In the deepest fields, >80% of the 2–10 keV cosmic X-ray background (CXB) has been resolved into individual objects (Hickox & Markevitch 2006; Brandt & Alexander 2015).

At X-ray energies above 10 keV, the observational picture is far less complete. Coded-mask instruments, such as *INTEGRAL* and *Swift*/BAT, have probed the demographics of hard X-ray emitting AGNs in the very local universe, to redshifts of $z \lesssim 0.1$ (Tueller et al. 2008; Beckmann et al. 2009). The fraction of the CXB resolved by these instruments at its peak intensity (20–30 keV) is ∼1% (Krivonos et al. 2007; Ajello et al. 2012; Vasudevan et al. 2013). Thus, until now, samples of AGNs selected at >10 keV, which are inherently less biased by obscuration than those at lower energy, could not be used to probe AGN demographics and, in particular, the evolution of highly obscured to Compton-thick ($N_{\rm H} \gtrsim \sigma_{\rm T}^{-1} \sim 10^{24}\,{\rm cm}^{-2}$) sources.

There is, therefore, strong motivation for extending sensitive X-ray surveys to high energy. Simple extrapolations of AGN populations detected by *Chandra* and *XMM-Newton* to higher energies based on average spectral properties fail to reproduce the shape and intensity of the CXB at 30 keV (e.g., Gilli et al. 2007). This indicates either that spectral models based on the small samples of high-quality 0.1–100 keV measurements used in CXB synthesis models fail to capture the true spectral complexity of AGNs, or that an additional highly obscured AGN population is present in the redshift range of $0 \lesssim z \lesssim 2$. It is likely that both factors are important at some level. A higher fraction of reflected emission than typically assumed, which hardens the emission above 10 keV, appear to be present in moderately obscured, $23 < \log(N_{\rm H}/{\rm cm}^{-2}) < 24$, AGNs (-Ricci et al. 2011). Even at moderate redshifts, reflection fractions are difficult to constrain with data restricted to <10 keV (e.g., Del Moro et al. 2014). In addition, it is difficult at low redshifts to properly measure high obscuring columns, which can lead to large errors in estimating intrinsic AGN luminosities (e.g., Lansbury et al. 2015). It is also challenging to identify Compton-thick objects in the range $0 \lesssim z \lesssim 2$ with the limited bandpass of *Chandra* and *XMM-Newton* (at $z \gtrsim 2$ these missions sample rest-frame energies above 20 keV). Thus both to characterize highly obscured AGNs and to constrain their evolution at $z \lesssim 2$ requires sensitive surveys at energies above 10 keV.

The *Nuclear Spectroscopic Telescope Array (NuSTAR)*, the first focusing high-energy X-ray (3–79 keV) telescope in orbit (Harrison et al. 2013), has been executing a series of extragalactic surveys as part of its core program, with the aim of measuring the demographics and properties of obscured AGNs. Through contiguous surveys in fields with existing multi-wavelength data combined with dedicated spectroscopic followup of sources serendipitously identified in individual fields, the *NuSTAR* extragalactic surveys have improved the sensitivity limits in the hard, 8–24 keV band by two orders of magnitude relative to *INTEGRAL* or *Swift*/BAT, and have probed a wide range in redshift, out to $z \gtrsim 2$.

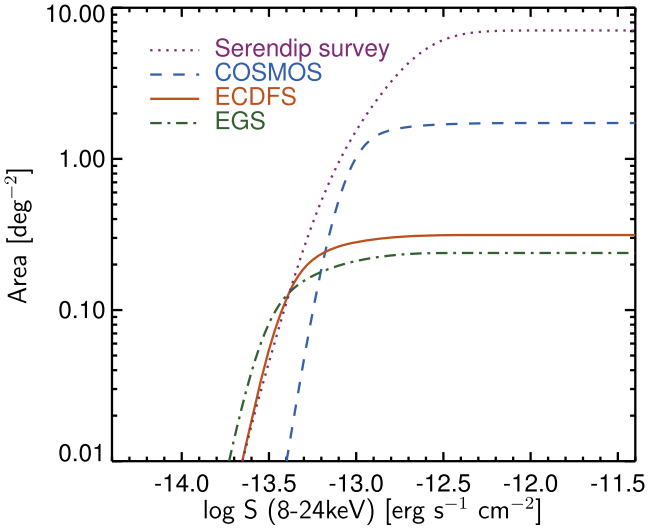

Figure 1. Area as a function of depth in the observed 8–24 keV band for the *NuSTAR* extragalactic surveys included in this work.

In this paper, we present the X-ray number counts ($\log N$–$\log S$) of AGNs, including the first sensitive measurements in the 8–24 keV band. We reach fluxes of S (8–24 keV) $\sim 3 \times 10^{-14}\,{\rm erg\,s^{-1}\,cm^{-2}}$, a factor of 100 deeper than previous measurements in this band. We compare the number counts to predictions from X-ray background synthesis models, and to extrapolations from *Chandra* and *XMM-Newton* surveys, and compare the intensity of resolved sources to that of the CXB. A companion paper (Aird et al. 2015a) presents direct constraints on the >10 keV AGN X-ray luminosity function. We adopt a flat cosmology with $\Omega_\Lambda = 0.7$ and $h = 0.7$, and quote 68.3% (i.e., 1σ equivalent) errors unless otherwise noted.

2. OBSERVATIONS AND DATA REDUCTION

For the results in this paper, we include all components of the *NuSTAR* extragalactic survey program that were completed and analyzed prior to 2015 March. This includes coverage of well-studied contiguous fields as well as identification and followup of sources serendipitously detected in all *NuSTAR* fields. Figure 1 shows the area as a function of depth for the survey components included in this work. At the shallow end, *NuSTAR* surveyed 1.7 deg^2 of the Cosmic Evolution Survey field (COSMOS; Scoville et al. 2007) to a depth of S (8–24 keV) $= 1.3 \times 10^{-13}\,{\rm erg\,s^{-1}\,cm^{-2}}$. The catalog and results from this survey are presented in Civano et al. (2015; hereafter C15). At the deep end, *NuSTAR* surveys have reached depths of S(8–24 keV) $= 2.5 \times 10^{-14}\,{\rm erg\,s^{-1}\,cm^{-2}}$ in the Extended *Chandra* Deep Field South (ECDFS; Lehmer et al. 2005) over an area of 0.3 deg^2 and in the deep *Chandra* region of the Extended Groth Strip (Goulding et al. 2012; Nandra et al. 2015) over an area of 0.23 deg^2. The ECDFS source catalog is presented in Mullaney et al. (2015; hereafter M15) and the EGS catalog will be presented in J. Aird et al. (2016, in preparation). The serendipitous survey

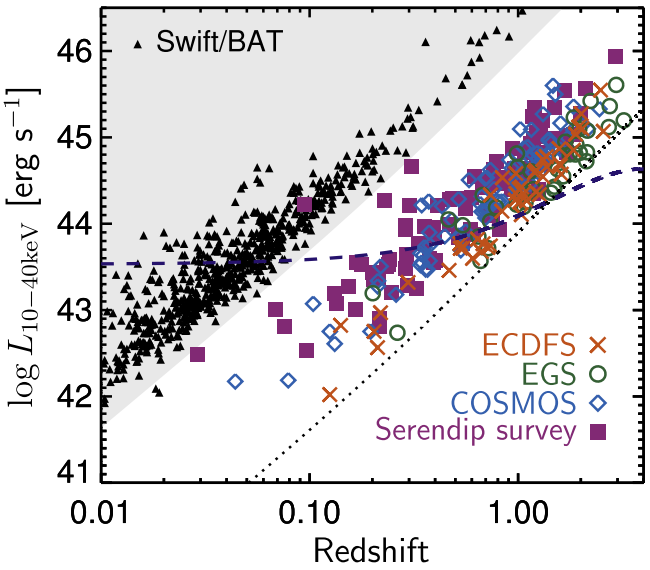

Figure 2. Rest-frame 10–40 keV X-ray luminosity versus redshift for the objects included in this work compared to sources in the *Swift*/BAT 70-month all-sky survey catalog (black triangles). The dashed line shows the location of the knee in the luminosity function from Aird et al. (2015b) as a function of redshift. The shaded region indicates the region of sensitivity of *Swift*/BAT, and the dotted line indicates the threshold for the *NuSTAR* surveys.

adopts a similar approach used with the *Chandra* SEXSI survey (Harrison et al. 2003), where fields are searched for point sources not associated with the primary target, and subsequent spectroscopic followup with the Keck, Palomar 200-in, *Magellan*, and NTT telescopes provides redshifts and AGN classifications. Preliminary results from this survey were published in Alexander et al. (2013), and the 30-month catalog and results will be published in G. Lansbury et al. (2016, in preparation).

The overall sample consists of 382 unique sources detected in the full (3–24 keV), soft (3–8 keV), or hard (8–24 keV) bands, of which 124 are detected in the hard band and 226 are detected in the soft band. Figure 2 shows the distribution of rest-frame 10–40 keV luminosity versus redshift for the sources in our sample. Luminosities in this plot are derived from the 8–24 keV count rates (if detected in that band) assuming an unabsorbed X-ray spectrum with a photon index $\Gamma = 1.8$ folded through the *NuSTAR* response. If the source is not detected in the 8–24 keV band, we calculate luminosities using the 3–24 keV or (if not detected at 3–24 keV) the 3–8 keV count rates. The median redshift for the entire *NuSTAR* sample is $\langle z \rangle = 0.76$, with a median luminosity of $\langle \log(L_{10-40\,\mathrm{keV}}/\mathrm{erg\ s^{-1}}) \rangle = 44.37$. For comparison, we plot the distribution of AGNs in the *Swift*/BAT 70-month catalog (Baumgartner et al. 2013). For reference, the dashed line in Figure 2 shows the location of the knee in the luminosity function as a function of redshift from the *Chandra*-based study of Aird et al. (2015b), extrapolated to the 10–40 keV band. Together, these surveys cover a broad range of luminosity and redshift.

2.1. Contiguous Survey Fields

We have adopted uniform source detection and flux extraction methodologies across the COSMOS, ECDFS, and EGS survey fields. For the ECDFS and COSMOS fields, we use the source lists and supporting data products (mosaic images, exposure maps, and background maps in the 3–24, 3–8, and 8–24 keV energy bands) from M15 and C15, respectively. We adopt exactly the same approach for the analysis of the EGS field (J. Aird et al. 2016, in preparation). We summarize the analysis approach here, and refer the reader to the relevant catalog papers for details.

For source detection, we convolve both the mosaic images and background maps with a 20″-radius aperture at every pixel, and determine the probability, based on Poisson statistics, that the total image counts are produced by a spurious fluctuation of the background. We generate the background maps based on the NUSKYBGD code (see Wik et al. 2014, for details). We then identify groups of pixels in these false probability maps, using SExtractor, where the probability is less than a set threshold. Different thresholds are used in each field and in each energy band based on the expected number of spurious sources in simulations (see C15, M15 and J. Aird et al. 2016, in preparation, for specific values used for each field). We merge detections in multiple bands to produce the final catalogs, which include 61 sources (3–8 keV) and 32 sources (8–24 keV) in COSMOS, 33 sources (3–8 keV) and 19 sources (8–24 keV) in ECDFS, and 26 sources (3–8 keV) and 13 sources (8–24 keV) in EGS. The detection thresholds are chosen to ensure the catalogs are 99% reliable, Thus, we expect very few spurious sources (see M15, C15).

Source confusion must be corrected for since blended sources result in the mis-estimation of source counts and fluxes. The *NuSTAR* PSF is relatively large compared to *Chandra* and *XMM-Newton*, and so source blending is particularly important to account for when comparing number counts from *NuSTAR* to these lower-energy, higher-resolution missions. The source de-blending procedure is described in detail in M15 and C15. To test the validity of the procedure, we performed Monte Carlo simulations, where source fluxes were drawn from a published number counts distribution, counts maps were simulated, and sources were extracted and de-blended. We then verified that the resulting number counts distribution matches the input. The details of these simulations are provided in Section 4 of C15.

2.2. Serendipitous Survey

The source-detection procedure for the serendipitous survey is the same as that outlined above, and described in detail in C15 and M15, though with a slightly different procedure for background determination. Many of the fields have bright central targets that contaminate a portion of the *NuSTAR* field of view. We thus take the original images and convolve them with an annular aperture of inner radius 30″ and outer radius 90″. We rescale the counts within this annulus to that of a 20″ radius region based on the ratio of the aperture areas and effective exposures. This procedure produces maps of the local background level at every pixel based on the observed images, and will thus include any contribution from the target object. We then use these background maps, along with the mosaic images, to generate false probability maps. From here, the source detection follows that used in the contiguous fields, using a false probability threshold of $<10^{-6}$ across all bands. We exclude any detections within 90″ of the target position, and also any areas occupied by large, foreground galaxies or known sources that are associated with the target (but are not at the aimpoint). We also exclude areas where the effective exposure is $<20\%$ of the maximal (on-axis) exposure in a given field. Any *NuSTAR* fields at Galactic latitudes $<20^{\circ}$ are

also excluded from our sample. Full details of the serendipitous survey program will be provided in G. Lansbury et al. (2016, in preparation), which will also indicate those serendipitous fields used in this work. In total, we include 106 serendipitous sources (3–8 keV) and 60 (8–24 keV).

3. NUMBER COUNT MEASUREMENTS

To determine the number counts ($\log N$–$\log S$), we adopt a Bayesian approach (see Georgakakis et al. 2008, Lehmer et al. 2012) that assigns a range of possible fluxes to a given source based on the Poisson distribution, which we then fold through the differential number counts distribution. We assume that the differential number counts are described by a single power-law function:

$$\frac{dN}{dS} = K\left(\frac{S}{10^{-13}\,\mathrm{erg\,s^{-1}\,cm^{-2}}}\right)^{\beta}, \quad (1)$$

where K is the normalization at $S = 10^{-13}$ erg s^{-1} cm^{-2} and β is the slope. Folding the Poisson likelihood for each individual source through the differential number counts given by Equation (1) accounts for the Eddington bias, allowing for the fact that a detection is more likely to be due to a positive fluctuation from a source of lower flux than vice versa. We limit the range of possible source fluxes to a factor of three below the nominal flux limit[29] to prevent the probability distribution from diverging at the faintest fluxes as a result of our assumed power-law function.

We optimize the values of the parameters describing the power-law model for the differential number counts by performing an unbinned maximum likelihood fit for all sources detected in a given band (see Georgakakis et al. 2008). We also estimate differential source number counts in a number of fixed-width bins in flux using the $N_{\rm obs}/N_{\rm mdl}$ method of Miyaji et al. (2001), as expanded on in Aird et al. (2010), to account for flux probability distributions. The binned estimate of the differential source number counts is then given by

$$\left[\frac{dN}{dS}\right]_{\rm bin} = \left[\frac{dN}{dS}\right]_{\rm mdl}\frac{N_{\rm obs}}{N_{\rm mdl}}, \quad (2)$$

where $\left[\frac{dN}{dS}\right]_{\rm mdl}$ corresponds to the power-law model for the differential number counts evaluated at the center of the bin, $N_{\rm mdl}$ is the predicted number of sources in a bin (found by folding the model through the sensitivity curve), and $N_{\rm obs}$ is the effective observed number of sources, allowing for the distribution of possible fluxes (thus, a single source can make a partial contribution to multiple bins). We estimate errors based on Poisson uncertainties in $N_{\rm obs}$ as given by Gehrels (1986).

Figure 3 (left) shows the resulting differential source number densities based on the *NuSTAR* samples from the four survey components combined, in the 3–8 keV band. We also compare the *NuSTAR* measurements to the best-fit broken power-law functions determined from *Chandra* surveys by Georgakakis et al. (2008) and a joint analysis of *XMM-Newton* and *Chandra* surveys by Mateos et al. (2008). We convert the *Chandra* (4–7 keV) and *XMM-Newton* (2–10 keV) number counts to match the 3–8 keV *NuSTAR* band assuming a $\Gamma = 1.8$ power-law X-ray spectrum. Because the bands are largely overlapping, the choice of photon spectral index does not significantly affect the results. To ease comparison between the different results, we have scaled dN/dS by the Euclidean slope, $S^{-2.5}$. The *NuSTAR* measurements constrain the slope well over the range of $-14 < \log\,(S/\mathrm{erg\,s^{-1}\,cm^{-2}}) < -12.5$. The best-fit values for the power-law parameters in this band are $\log K = 13.84 \pm 0.04$, $\beta = -2.81 \pm 0.08$.

The *NuSTAR* results generally agree with *Chandra* and *XMM-Newton;* though, the slope of the number counts with flux is somewhat steeper. Below $S \sim 10^{-14}$ erg s^{-1} cm^{-2}, the *NuSTAR* measurements are poorly constrained, so that the location of the break in the number counts seen by *Chandra* and *XMM-Newton* cannot be independently confirmed. The difference in slope of the number counts with flux between *NuSTAR* and the soft X-ray telescopes is due the different instrument responses and the corresponding uncertainties in converting count rates to fluxes based on simple spectral models. To verify this, we folded the population synthesis model of Aird et al. (2015b) through the *NuSTAR* response function to predict the observed count-rate distribution. We convert the count rates to fluxes, applying our standard count rate to flux conversion factor. We repeated this exercise adopting the *Chandra* response function, applying the count rate to flux conversion factor from Georgakakis et al. (2008). For moderately to heavily absorbed sources ($N_{\rm H} \sim 10^{23}$ cm^{-2}), the expected count rates are more strongly suppressed using the *Chandra* response (because the *NuSTAR* instrument response is more strongly weighted to higher energies). The intrinsic fluxes are therefore underestimated for such sources with *Chandra* when a single conversion factor is assumed. We have verified that this effect leads to a slope difference in the expected $\log N$–$\log S$ at $f_{3-8\rm keV} \sim 10^{-14}$–$10^{-13}$ erg s^{-1} cm^{-2} that matches the discrepancy seen between the *NuSTAR* measurements and the *Chandra* and *XMM-Newton* measurements shown in Figure 3 (left). Figure 4 (left) shows the integral number counts in the 3–8 keV band.

Figure 3 (right) shows the differential source number counts in the 8–24 keV band, along with the best-fit power law, parametrized by $\log K = 14.3 \pm 0.04$, and $\beta = -2.76 \pm 0.10$. We also plot extrapolations of the Mateos et al. (2008) *Chandra*+ *XMM-Newton* counts and the Georgakakis et al. (2008) *Chandra* counts to the harder, largely non-overlapping 8–24 keV band (dotted and solid lines in Figure 3). The dotted line shows the extrapolation assuming $\Gamma = 1.8$, which is typical of unabsorbed AGNs, and systematically under-predicts the *NuSTAR* measurements. Using a maximum likelihood analysis, we find that a spectral photon index of $\Gamma = 1.48$ (solid line) provides the best match between the extrapolation of the Georgakakis et al. (2008) model and the *NuSTAR* data, indicating that a substantial population of absorbed and/or hard-spectrum sources is required to reproduce the *NuSTAR* measurements.

4. COMPARISON WITH THE *SWIFT*/BAT LOCAL AGN SAMPLE

In combination, *NuSTAR* and *Swift*/BAT sample the hard X-ray AGN population over a wide range in flux and redshift. *Swift*/BAT has measured the number counts at fluxes of $S \gtrsim 3 \times 10^{-12}$ erg s^{-1} cm^{-2} in the 15–55 keV band for the local ($z \lesssim 0.1$) AGN sample (Ajello et al. 2012). Although

[29] We note that allowing for a source flux that is a factor 10 or more below the nominal flux limit has a neglible impact on our results.

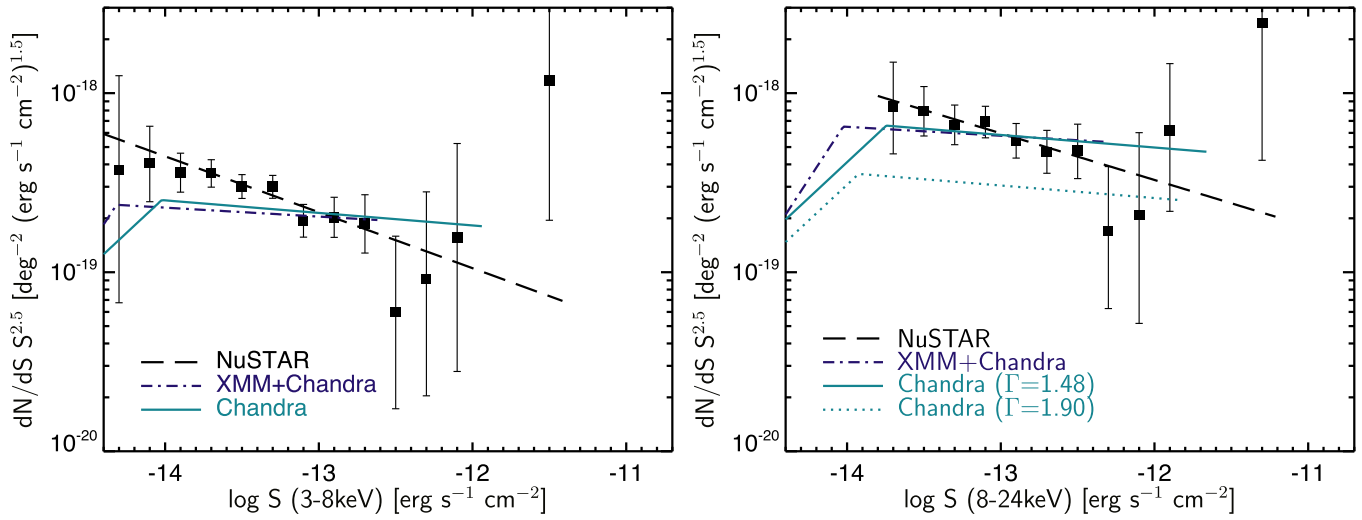

Figure 3. Left panel: the differential number counts for the observed 3–8 keV band. The data points (black squares) show measurements from the combined *NuSTAR* survey fields, where error bars are 1σ equivalent (i.e., 68.3% confidence level), and the black dashed line shows the best-fit power law. The solid line shows the best fit to the number counts as measured by *Chandra* (Georgakakis et al. 2008), and the dotted–dashed line shows the best fit from a combined analysis of *XMM-Newton* and *Chandra* data (Mateos et al. 2008). Right panel: the differential log *N*–log *S* in the 8–24 keV band (black squares). The solid blue line and dotted–dashed lines show the *Chandra* (4–7 keV) and *XMM-Newton* measurements extrapolated to the 8–24 keV band using a photon power-law index of $\Gamma = 1.48$. The blue dotted line shows the *Chandra* measurements using a steeper ($\Gamma = 1.9$) power law for the spectral extrapolation.

there is a gap in the flux range probed by BAT and the $S \lesssim 3 \times 10^{-13}$ erg s^{-1} cm^{-2} population probed by *NuSTAR*, extrapolating the BAT differential number counts to fainter fluxes indicates whether there is any evolution between the low-redshift BAT AGN population and the higher-redshift *NuSTAR* sources.

Figure 5 shows the *NuSTAR* 8–24 keV number counts together with the BAT measurements from Ajello et al. (2012), which are well described by a single power-law dN/dS with slope $\beta \approx 2.5$ (bold dashed line). We have converted the BAT 15–55 keV fluxes to the 8–24 keV band assuming a photon index of $\Gamma = 1.7$, the value that provides the best fit to the average BAT AGN spectral model from Burlon et al. (2011). The hatched region indicates the measurement uncertainties from Ajello et al. (2012), showing that the formal error is small, about the width of the dashed line. It is clear that the extrapolation of the BAT counts to lower fluxes where the counts are well-constrained by *NuSTAR* ($f \sim 10^{-13.5}$ erg s^{-1} cm^{-2}) significantly under-predicts the *NuSTAR* measurements. This disagreement is not surprising, since there is strong evolution in the AGN population between the local ($z \sim 0.1$) BAT sample and the higher-redshifts probed by *NuSTAR*.

5. COMPARISON WITH X-RAY BACKGROUND SYNTHESIS MODELS

The existence of a population of obscured and Compton-thick objects beyond those directly resolved below 10 keV has long been postulated by CXB synthesis models. These models reproduce the hard spectrum of the CXB using measured AGN X-ray luminosity functions (XLFs), which are well constrained (except in the very local universe) only below 10 keV, together with models for the broadband (∼1–1000 keV) AGN spectra and estimates of the Compton-thick AGN fraction and its evolution (e.g., Gilli et al. 2007, Treister et al. 2009, Ueda et al. 2014). The XLF measurements, assumptions about AGN spectral evolution, and Compton-thick fractions differ significantly among models.

Figure 5 compares the *NuSTAR* counts to three different CXB synthesis models: the model from Gilli et al. (2007; dashed line with circles), the model of Ueda et al. (2014), and an an updated version of the Ballantyne et al. (2011) model. The details of the Gilli et al. (2007) and Ueda et al. (2014) models are documented in the relevant publications. The updated Ballantyne model differs from Ballantyne et al. (2011) in that it uses the new Ueda et al. (2014) luminosity function, a better spectral model from Ballantyne (2014), the Burlon et al. (2011) N_H distribution, and the redshift evolution and obscured fraction from Ueda et al. (2014). Other aspects, including the normalization of the Compton-thick fraction are the same as in Ballantyne et al. (2011). We include this model because it fits the CXB spectrum even after including the effects of blazers.

All three models are in good agreement with the measured *NuSTAR* counts. However, all of the models lie significantly above the *Swift*/BAT measurements at $S \gtrsim 10^{-11.5}$ erg s^{-1} cm^{-2}. The discrepancy between the BAT measurements and the models cannot be accounted for by uncertainties in the spectral shape; a spectral index of $\Gamma = 2.1$ when converting to the 8–24 keV band is required to make the *Swift*/BAT 15–55 keV measurements agree with the model predictions. This is significantly softer than the average measured spectral shape, even for unobscured AGNs, and can thus be ruled out. Therefore, this discrepancy appears to be due to evolution in the hard XLF, absorption distribution, or spectral properties of AGNs between the very local *Swift*/BAT sample and the more distant ($z \sim 0.5$–1) *NuSTAR* sample that is not fully accounted for in these population synthesis models (see also Aird et al. 2015b).

6. SUMMARY AND CONCLUSIONS

We have presented measurements of the number counts of AGN with *NuSTAR* in two bands, from 3–8 keV and 8–24 keV. The data span a broad range in flux, with good constraints covering $10^{-14} \lesssim S$(8–24 keV; erg s^{-1} cm^{-2}) $\lesssim 10^{-13}$. The 3–8 keV differential source number densities are in agreement with measurements from *Chandra* and *XMM-Newton;* though,

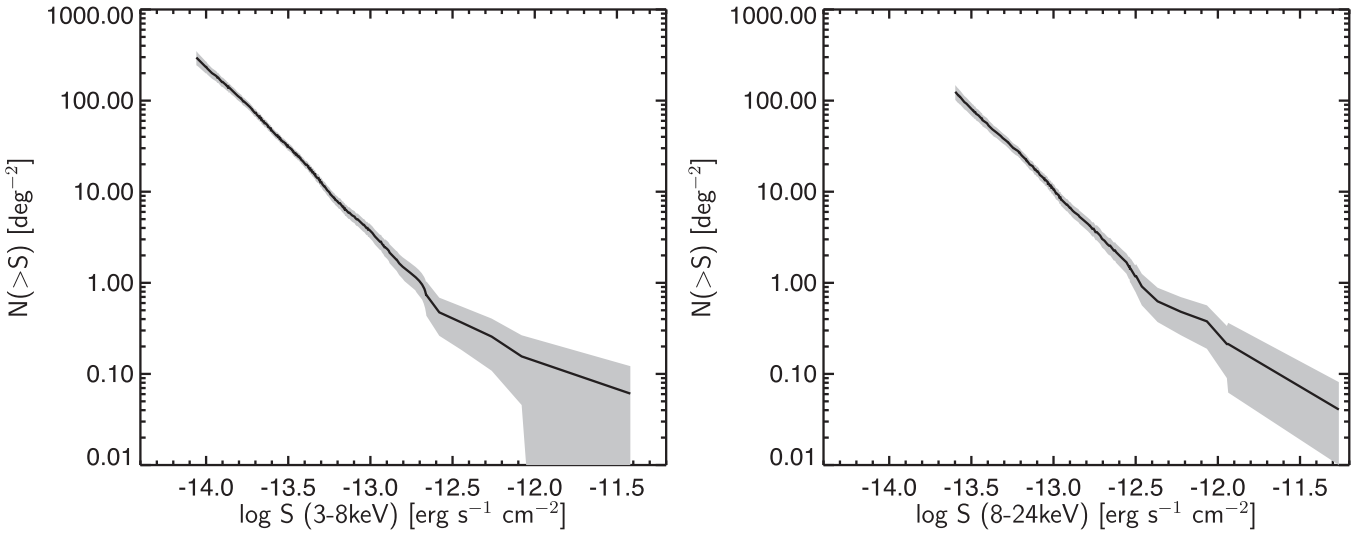

Figure 4. Integral number counts for the 3–8 keV (left) and 8–24 (right) observed bands. The gray shaded region shows the 68.3% confidence region on the integrated number counts based on the Poisson error in the number of sources weighted by the survey area as a function of flux. The blue line on the left plot shows a comparison to *Chandra* counts extrapolated from 4–7 keV.

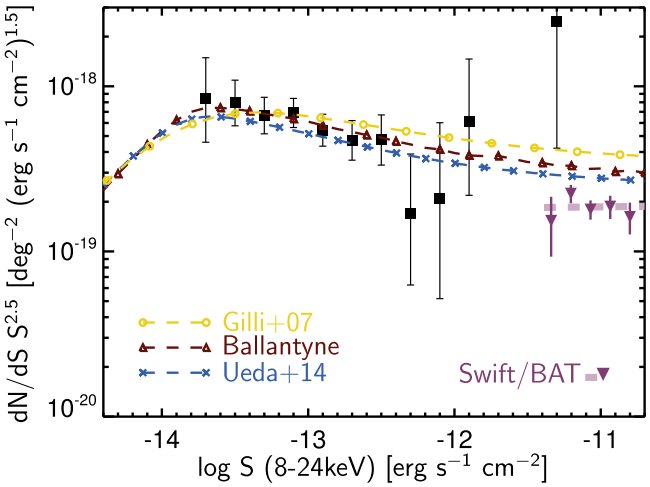

Figure 5. *NuSTAR* 8–24 keV number counts compared to *Swift*/BAT (bold dashed line; Ajello et al. 2012). The hatched region indicates the uncertainty in the overall fit from Ajello et al. (2012). We convert the BAT 15–55 keV band to the 8–24 keV band using a power law with photon index $\Gamma = 1.7$ (the best-fit to the average BAT AGN spectrum in the 15–55 keV band). The dashed line with triangles shows predictions from the CXB synthesis model of Ballantyne 2011 updated to use the Ueda 2014 luminosity function. The dashed line with crosses shows the population synthesis model from Ueda et al. (2014). The dashed line with circles shows predictions from the CXB model from Gilli et al. (2007). The plotted errors are 1σ.

the slope measured by *NuSTAR* is somewhat steeper. The slope difference results from the fact that the *NuSTAR* effective area curve is weighted to significantly higher energies compared to *XMM-Newton* and *Chandra*, which results in the observed discrepancy when using a simple counts to flux conversion factor.

In the 8–24 keV band, we present the first direct measurement of the AGN number counts that includes data above ~10 keV and reaches down to flux levels $\sim 3 \times 10^{-14}$ erg s^{-1} cm^{-2}. In order to match the *NuSTAR* number counts, the flux measurements from *Chandra* and *XMM-Newton* must be extrapolated to higher energy using a spectrum with photon index $\Gamma = 1.48$. This photon index is significantly harder than the $\Gamma = 1.7$–1.9 that characterizes the unobscured AGN population and is also significantly harder than the average spectral index that characterizes the *Swift*/BAT AGN sample.

The *NuSTAR* number counts are in good agreement with predictions from population synthesis models that explain the hard spectrum of the CXB using different assumptions about obscuration, the Compton-thick sample, and the spectra shape of AGN in the hard X-ray band (see Figure 5). This directly confirms the existence of a population of AGNs with harder spectra than those typically measured below 10 keV. The spectral hardness could be due either to increased reflection or near Compton-thick absorption. The updated Ballantyne model, for example, uses an AGN spectral model with a strong Compton reflection component with a relative normalization component of $R = 1.7$. Our measurements of the rest-frame 10–40 keV XLF Aird et al. (2015a) also indicate that a significant population of AGNs with hard X-ray spectra is required to reconcile our *NuSTAR* data with prior, lower-energy XLF measurements. To what extent this results from obscuration versus higher levels of reflection will be determined by the spectral analysis of *NuSTAR* sources in the survey fields (A. Del Moro et al. 2016, in preparation, L. Zappacosta et al. 2016, in preparation), and from spectral modeling of high quality data from local AGN samples (M. Baloković et al. 2016, in preparation).

The *NuSTAR* 8–24 keV number counts lie significantly above a direct extrapolation with flux of the number counts at brighter fluxes, sampled by the *Swift*/BAT survey in the 15–55 keV band (Figure 5). This discrepancy is not surprising given the known evolution of the AGN population between the low redshift *Swift*/BAT AGNs and the higher-redshift *NuSTAR* sample It is interesting that the BAT data are in tension with CXB synthesis models (see Figure 5), which are in good agreement with the *NuSTAR* measurements. The most natural explanation for the difference is an evolution in the hard XLF, absorption distribution, or spectral properties of AGNs between the very local objects seen by BAT and the more distant ($z \sim 0.5$–1) *NuSTAR* sample that is not accounted for in the current population synthesis models.

Table 1 provides CXB fluxes measured by hard X-ray instruments in the 20–50 keV and 8–24 keV bands. To convert

Table 1
X-ray Background Measurements

Instrument	I_{CXB} (20–50 keV)	I_{CXB} (8–24 keV)	% resolved by *NuSTAR*
HEAO-1 A2 + A4	6.06 ± 0.06	6.33 ± 0.07	39
HEAO-1 A2	5.60 ± 0.30	6.27 ± 0.33	39
BeppoSAX	5.89 ± 0.19	6.48 ± 0.21	38
INTEGRAL	~6.66	7.33	33
BAT	6.50 ± 0.15	7.16 ± 0.17	34

Note. CXB intensity (I_{CXB}) is given in units of 10^{-8} ergs cm^{-2} s^{-1} sr^{-1}. Intensities in the 20–50 keV band are taken from Gruber et al. (1999) for *HEAO-1* A2 + A4, Marshall et al. (1970) for *HEAO-1* A2, Frontera et al. (2007) for *BeppoSAX*, Churazov et al. (2007) for *INTEGRAL*, and Ajello et al. (2008) for *BAT*.

the intensities to the 8–24 keV band for those instruments that do not cover this energy range (*BeppoSAX, INTEGRAL, Swift*/BAT), we used Equation (5) of Ajello et al. (2008), which parametrizes the CXB spectrum between 2 keV and 2 MeV based on a fit to available data. The *NuSTAR* extragalactic surveys have reached depths of $S(8\text{–}24\,\mathrm{keV}) \approx 3 \times 10^{-14}$ erg s^{-1} cm^{-2}. Comparing to the total integrated flux of the CXB as measured by collimated and coded aperture instruments shown in Table 1, this corresponds to a resolved fraction of 33%–40% in the 8–24 keV band (Figure 6), with an additional statistical uncertainty of 5%. Even for the highest measured CXB flux from Churazov et al. (2007) *NuSTAR* still resolves 33%, which is a significant advance compared to the 1%–2% resolved to-date by coded-mask instruments above 10 keV (Krivonos et al. 2007; Vasudevan et al. 2013).

The resolved fraction of the CXB we measure is in good agreement with pre-launch predictions based on CXB synthesis models (Ballantyne et al. 2011). At the current depth, the *NuSTAR* surveys do not probe the break in the number counts distribution expected, based on extrapolations from *Chandra* and *XMM-Newton*, to occur at S (8–24 keV) $\sim 10^{-14}$ erg s^{-1} cm^{-2}. Reaching these depths will be challenging because the deep fields are currently background dominated, such that sensitivity improves only as the square root of observing time improves. However, additional exposure in the ECDFS is planned, along with expansion of the deep surveys to cover the CANDELS/UDS field (Grogin et al. 2011; Koekmoer et al. 2011), and continuation of the serendipitous survey, which will better constrain the slope of the number counts distribution above the break and improve spectral constraints on the resolved AGN population.

This work was supported under NASA Contract No. NNG08FD60C, and made use of data from the *NuSTAR* mission, a project led by the California Institute of Technology, managed by the Jet Propulsion Laboratory, and funded by the National Aeronautics and Space Administration. We thank the *NuSTAR* Operations, Software and Calibration teams for support with the execution and analysis of these observations. This research has made use of the *NuSTAR* Data Analysis Software (NuSTARDAS) jointly developed by the ASI Science Data Center (ASDC, Italy) and the California Institute of Technology (USA). J.A. acknowledges support from ERC Advanced Grant FEEDBACK at the University of Cambridge and a COFUND Junior Research Fellowship from the Institute of Advanced Study, Durham University.

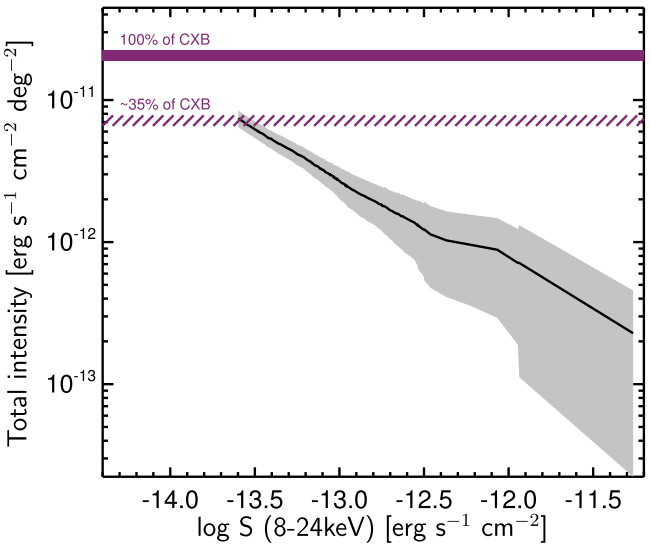

Figure 6. Total intensity as a function of 8–24 keV flux of the resolved sources in the sample included in this work. The horizontal lines indicate 35% (hatched line) and 100% (solid line) of the cosmic X-ray background (CXB). The width of the lines indicates the range of normalizations determined by different instruments (see Table 1 for references). At the faint end of the surveys included here, *NuSTAR* is resolving ~35% of the CXB.

REFERENCES

Aird, J., Alexander, D., Ballantyne, D., Civano, F., & Mullaney, J. 2015a, ApJ, 815, 66
Aird, J., Coil, A. L., Georgakakis, A., et al. 2015b, MNRAS, 451, 1892
Aird, J., Nandra, K., Laird, E. S., et al. 2010, MNRAS, 401, 2531
Ajello, M., Alexander, D. M., Greiner, J., et al. 2012, ApJ, 749, 21
Ajello, M., Greiner, J., Sato, G., et al. 2008, ApJ, 689, 666
Alexander, D. M., Stern, D., Del Moro, A., et al. 2013, ApJ, 773, 125
Ballantyne, D. R. 2014, MNRAS, 437, 2845
Ballantyne, D. R., Draper, A. R., Madsen, K. K., Rigby, J. R., & Treister, E. 2011, ApJ, 736, 56
Baumgartner, W. H., Tueller, J., Markwardt, C. B., et al. 2013, ApJS, 207, 19
Beckmann, V., Soldi, S., Ricci, C., et al. 2009, A&A, 505, 417
Brandt, W. N., & Alexander, D. M. 2015, A&ARv, 23, 1
Burlon, D., Ajello, M., Greiner, J., Comastri, A., Merloni, A., & Gehrels, N. 2011, ApJ, 728, 58
Churazov, E., Sunyaev, R., Revnivtsev, M., et al. 2007, A&A, 467, 529
Civano, F., Hickox, R. C., Puccetti, S., et al. 2015, ApJ, 808, 185
Del Moro, A., Mullaney, J. R., Alexander, D. M., et al. 2014, ApJ, 786, 16
Di Matteo, T., Colberg, J., Springel, V., Hernquist, L., & Sijacki, D. 2008, ApJ, 676, 33
Frontera, F., Orlandini, M., Landi, R., et al. 2007, ApJ, 666, 86
Gehrels, N. 1986, ApJ, 303, 336
Georgakakis, A., Nandra, K., Laird, E. S., Aird, J., & Trichas, M. 2008, MNRAS, 388, 1205
Gilli, R., Comastri, A., & Hasinger, G. 2007, A&A, 463, 79
Goulding, A. D., Forman, W. R., Hickox, R. C., et al. 2012, ApJS, 202, 6
Grogin, N. A., Kocevski, D. D., Faber, S. M., et al. 2011, ApJS, 197, 35
Gruber, D. E., Matteson, J. L., Peterson, L. E., & Jung, G. V. 1999, ApJ, 520, 124
Harrison, F. A., Eckart, M. E., Mao, P. H., Helfand, D. J., & Stern, D. 2003, ApJ, 596, 944
Harrison, F. A., Craig, W. W., Christensen, F. E., et al. 2013, ApJ, 770, 103
Hickox, R. C., & Markevitch, M. 2006, ApJ, 645, 95
Koekemoer, A. M., Faber, S. M., Ferguson, H. C., et al. 2011, ApJS, 197, 36
Krivonos, R., Revnivtsev, M., Lutovinov, A., Sazonov, S., Churazov, E., & Sunyaev, R. 2007, A&A, 475, 775
Lansbury, G. B., Gandhi, P., Alexander, D. M., et al. 2015, ApJ, 809, 115
Lehmer, B. D., Brandt, W. N., Alexander, D. M., et al. 2005, ApJS, 161, 21
Lehmer, B. D., Xue, Y. Q., Brandt, W.N., et al. 2012, ApJ, 752, 46

Lumb, D. H., et al. 2002, A&A, 389, 93
Marshall, F., Boldt, E. A., Holt, S. S., et al. 1970, ApJ, 235, 4
Mateos, S., Warwick, R. S., Carrera, F. J., et al. 2008, AAP, 492, 51
Merloni, A., & Heinz, S. 2008, MNRAS, 388, 1011
Miyaji, T., Hasinger, G., & Schmidt, M. 2001, A&A, 369, 49
Mullaney, J. R., Del-Moro, A., Aird, J., et al. 2015, ApJ, 808, 184
Nandra, K., Laird, E. S., Aird, J. A., et al. 2015, ApJS, 220, 10
Ricci, C., Walter, R., Courvoisier, T. J.-L., & Paltani, S. 2011, A&A, 532, A102
Scoville, N., Aussel, H., Brusa, M., et al. 2007, ApJS, 172, 1
Soltan, A. 1982, MNRAS, 200, 115
Treister, E., Urry, C. M., & Virani, S. 2009, ApJ, 696, 110
Tueller, J., Mushotzky, R. F., Barthelmy, S., et al. 2008, ApJ, 681, 113
Ueda, Y., Akiyama, M., Hasinger, G., Miyaji, T., & Watson, M. G. 2014, ApJ, 786, 104
Vasudevan, R. V., Mushotzky, R. F., & Gandhi, P. 2013, ApJL, 770, L37
Wik, D. R., Hornstrup, A., Molendi, S., et al. 2014, ApJ, 792, 48
Yu, Q., & Tremaine, S. 2002, MNRAS, 335, 965